

First-Return Statistics in Henyey–Greenstein Scattering: Colored Motzkin Polynomials and the Cauchy Kernel

C Zeller¹ and R Cordery²

¹Claude Zeller Consulting LLC, Tillamook, Oregon 97134, USA

²Department of Physics, Fairfield University, Fairfield, Connecticut 06824, USA

czeller@ieee.org, rcordery@fairfield.edu

Abstract

We show that first-return statistics in three-dimensional Henyey–Greenstein scattering are governed by colored Motzkin polynomials modulated by a Cauchy kernel. In our previous work [7], we established that first-return probabilities in 1D scattering expand in Catalan and Motzkin numbers. Extending this to 3D anisotropic scattering requires a Boundary Truncation Factor (BTF) that, as Monte Carlo suggested, takes a Cauchy kernel form. Here we explain why.

Projecting the 3D walk onto the depth–optical-path plane and applying the Central Limit Theorem yields Gaussian statistics; Beer–Lambert weighting shifts the Gaussian center linearly in scattering order n , producing a Cauchy-distributed ratio:

$$\text{BTF}(n, g) = \frac{A(g)}{1 + [(n - 2)/m_*(g)]^2}$$

with $m_*(g) = 4g/(1-g)$ and $A(g) = 1 - g(1+g)/2$. Monte Carlo confirms this to 1–2% for $g < 2/3$. The integers 2 and 4 have geometric meaning: $n = 2$ is the minimum scattering order for first return; the factor 4 combines exponential path-length statistics with first-passage geometry.

New contributions beyond [7] include: (i) a projection formalism mapping 3D walks to two-dimensional phase space, (ii) a Central Limit Theorem derivation of the Cauchy BTF with explicit parameters, (iii) identification of a Poisson–Cauchy correspondence linking boundary-constrained exponential processes to heavy-tailed statistics, and (iv) generalization to oblique incidence through colored (two-color) Motzkin polynomials incorporating transverse activity. The closed-form BTF enables rapid reflectance computation without full Monte Carlo simulation, offering orders-of-magnitude speed-up for iterative inverse problems in tissue optics and material characterization.

Keywords: first-passage problem, random walk, Cauchy kernel, colored Motzkin polynomials, radiative transfer, Henyey–Greenstein scattering

1 Introduction

First-passage problems appear throughout statistical mechanics—in polymer physics, diffusion-limited aggregation, financial mathematics, and queueing theory [1, 2, 3]. A clean example arises in radiative transport: photons entering a scattering medium execute a three-dimensional random walk and may return to the entry boundary. The statistics of this first-passage event encode how stochastic motion interacts with geometric constraint.

Throughout this paper, we use “first-return” to mean first passage back to the entry boundary ($z = 0$) from the interior ($z > 0$) with negative z -velocity—that is, the photon must be traveling outward when it crosses the boundary. This distinction matters because trajectories grazing the boundary while moving inward do not contribute to reflectance.

In our previous work in this journal [7], we established that first-return probabilities in one-dimensional isotropic scattering expand in Catalan numbers, the combinatorial objects counting Dyck paths. The reflectance of a semi-infinite Kubelka–Munk medium [9] admits the generating function representation

$$R_\infty(S, \chi) = \frac{1}{2} \cdot \frac{S}{S + \chi} \cdot C\left(\frac{S^2}{4(S + \chi)^2}\right) \quad (1)$$

where $C(x) = \sum_{n=0}^{\infty} C_n x^n$ is the Catalan generating function [20] and $C_n = (2n)!/(n!(n+1)!)$. This result is distribution-free—it depends only on the alternating (zigzag) structure of the projected walk, not on step-length distributions. Exactness here refers to conditional equivalence under the sole assumptions of Poisson-distributed scattering events and Markovian angular redistribution; no further closure or approximation is introduced. We further showed that forward-peaked scattering introduces “flat” steps in the combinatorial language: scattering events that preserve the sign of the axial velocity component. The natural generalization from Catalan to Motzkin structures [17, 18] accommodates this extension, with the first-return probability becoming

$$P_{\text{refl}}^{(1D)}(n, r) = M_{n-2} \left(\frac{1-2r}{r} \right) \cdot \left(\frac{r}{2} \right)^{n-1} \quad (2)$$

where $M_n(t)$ is the Motzkin polynomial and r the backward-step probability.

The central challenge is extending this framework to *three-dimensional anisotropic* scattering governed by the Henyey–Greenstein phase function [14]. Direct embedding of Motzkin structure via an effective backscattering coefficient $r_b(g)$ fails; Monte Carlo studies [8] show the mapping requires a **Boundary Truncation Factor** (BTF) that accounts for geometric constraints at the boundary.

We show that the BTF follows a **Cauchy kernel** in the scattering order n :

$$\text{BTF}(n, g) = \frac{A(g)}{1 + \left(\frac{n-n_0}{m_*(g)}\right)^2} \quad (3)$$

with parameters expressible in terms of the anisotropy factor g alone:

$$m_\star(g) = \frac{4g}{1-g} \quad (\text{width}) \quad (4)$$

$$A(g) = 1 - \frac{g(1+g)}{2} \quad (\text{amplitude}) \quad (5)$$

$$n_0 = 2 \quad (\text{peak location}) \quad (6)$$

The theory applies for $g \lesssim 2/3$ and $n \geq 2$; above $g \approx 2/3$, deviations grow gradually. The simple integer coefficients (2, 4) suggest underlying mathematical structure rather than empirical fitting; this paper provides that foundation.

While Poisson transport and first-passage problems have been studied independently, their explicit identification as the mechanism enforcing exact dimensional reduction has not been previously articulated.

1.1 Relation to previous work

This paper is the second in a series developing the combinatorial theory of radiative first-passage problems. Table 1 summarizes the progression.

Table 1: Progression of results from [7] through the present work.

Aspect	Zeller & Cordery (2020)	Present work
Dimension	1D	3D \rightarrow 1D projection
Scattering	Isotropic + forward bias	Henyey–Greenstein
Combinatorics	Catalan \rightarrow Motzkin	Colored Motzkin + BTF
BTF	Not needed	Derived (Cauchy)
Incidence	Normal only	Normal + oblique
Key result	Equation (2)	Equations (3), (55)

From our 2020 paper, we carry forward: (i) the Motzkin polynomial framework (equation 2); (ii) the distribution-free character of first-passage combinatorics; and (iii) the connection to classical fluctuation theory [5, 4]. What is new here is: (i) the projection formalism mapping 3D walks to the (z, τ) plane; (ii) the Central Limit Theorem analysis establishing Gaussian statistics; (iii) the saddle-point mechanism explaining why the BTF is necessarily Cauchy; (iv) derivation of the specific parameters $m_\star(g)$ and $A(g)$; and (v) generalization to oblique incidence via colored Motzkin polynomials.

An empirical version of this framework, with Monte Carlo-calibrated BTF, appeared in [8]. That work established the Cauchy kernel through model selection but left the mathematical origin unexplained. The present paper provides the theoretical foundation.

1.2 Connection to statistical mechanics

The Cauchy kernel is the $\alpha = 1$ stable law—the only symmetric stable law besides the Gaussian [6, 23]. Its appearance here is not accidental.

When Poisson processes on the line are subjected to boundary constraints and ratio operations, they generically produce Cauchy-distributed quantities. In our problem: scattering events form a Poisson process generating exponential path lengths; the boundary constraint (first passage at $z = 0$) creates a ratio structure; and the BTF inherits the Cauchy kernel. The renewal property is not postulated, but follows directly from the memoryless nature of the underlying Poisson process governing free paths.

This links to Lévy flights, anomalous diffusion [26], and random walk resolvents—all of which show Cauchy signatures near boundaries [21, 22].

1.3 Comparison with generalized Kubelka–Munk

Our approach differs from previous 3D extensions of Kubelka–Munk. Sandoval and Kim [11, 12] extended KM through double spherical harmonics (DP_1), obtaining an 8×8 system for forward and backward power flow. For isotropic scattering in optically thick media, their generalized KM achieves errors below 15% when $z_0 \geq 10$ (where z_0 is the optical thickness).

However, DP_1 encounters difficulties for anisotropic scattering. Its basis functions contain only first-order azimuthal harmonics and cannot capture forward-peaked phase functions. At $g = 0.8$, Sandoval and Kim found errors exceeding 80% in transmitted power; at higher anisotropy, the approximation gives negative intensities.

The BTF framework inverts the dimensional strategy: instead of enriching 1D equations with 3D coupling, we project 3D angular physics onto 1D combinatorics and correct for boundary truncation. Table 2 compares the two approaches.

Table 2: Comparison of dimensional reduction strategies for semi-infinite media.

Property	gKM (Sandoval & Kim)	BTF (this work)
Geometry	Finite slab	Semi-infinite
Strategy	$1D \rightarrow 3D$ extension	$3D \rightarrow 1D$ projection
Angular basis	DP_1 (4 func./hemisphere)	HG sampling + Motzkin
Isotropic limit	<15% error for $z_0 \geq 10$	Recovers Catalan structure
Anisotropic range	$g \lesssim 0.5$ (qualitative)	$g < 2/3$ (<2% deviation)
High- g behavior	Unphysical (negative values)	Predictable drift
Incidence	Oblique via eigenmode	Oblique via colored Motzkin
Computational form	8×8 PDE system	1D polynomial evaluation

Practitioner guidance. For semi-infinite media with $g \lesssim 2/3$, the BTF+Motzkin method is both more accurate and computationally cheaper than DP_1 : it reduces to 1D polynomial evaluation rather than an 8×8 PDE system, achieving sub-2% accuracy versus 15% or worse for gKM. For finite slabs, strong absorption, or the most demanding oblique-incidence applications, generalized Kubelka–Munk or full Monte Carlo may still be preferred. The BTF framework is particularly advantageous in iterative inverse problems—such as extracting optical properties from diffuse reflectance measurements—where transport calculations must be repeated thousands of times per optimization run.

1.4 Paper organization

Section 2 reviews the 1D Motzkin framework [7]. Section 3 introduces the Boundary Truncation Factor—what it is, how it was discovered empirically, and why its Cauchy kernel demands explanation. Sections 4–7 provide that explanation: projection formalism, Central Limit Theorem, saddle-point analysis, and parameter derivation. Section 8 describes Monte Carlo validation. Section 9 places the result in the context of stable distributions. Section 10 presents the computational algorithm. Section 11 extends the framework to oblique incidence via colored Motzkin polynomials. Section 12 concludes.

2 One-dimensional theory: Catalan and Motzkin structures

In this section, we briefly review results from [7]; see [1, 2] for background.

2.1 Kubelka–Munk reflectance and Catalan numbers

The Kubelka–Munk equations [9, 13] describe one-dimensional radiative transport with isotropic scattering:

$$\begin{pmatrix} dI \\ dJ \end{pmatrix} = \begin{pmatrix} -(S + \chi) & S \\ -S & (S + \chi) \end{pmatrix} \begin{pmatrix} I \\ J \end{pmatrix} dz \quad (7)$$

where I and J are forward and backward fluxes, S the scattering coefficient, and χ the absorption coefficient. The reflectance of a semi-infinite slab is

$$R_\infty(S, \chi) = \frac{S + \chi}{S} - \sqrt{\left(\frac{S + \chi}{S}\right)^2 - 1} \quad (8)$$

The key result of [7] is that this reflectance expands in Catalan numbers:

$$R_\infty(S, \chi) = \sum_{n_p=1}^{\infty} \frac{C_{n_p-1}}{2^{2n_p-1}} \left(\frac{S}{S + \chi}\right)^{2n_p-1} \quad (9)$$

The combinatorial interpretation is that photon trajectories form alternating (zigzag) random walks, and first passage occurs when the walk first crosses $z = 0$ traveling backward. The probability of first passage at the n_p -th peak is $P(n_p) = C_{n_p-1}/2^{2n_p-1}$. This connects to fluctuation theory through Spitzer’s identity [3] and Andersen’s equivalence principle [5].

2.2 Motzkin extension for forward scattering

Catalan numbers count Dyck paths—walks restricted to up- and down-steps. Forward scattering introduces flat steps (events preserving the sign of z -velocity), requiring the Motzkin extension [17, 18, 19].

Definition (Motzkin polynomial). The Motzkin polynomial of degree n is

$$M_n(t) = \sum_{k=0}^{\lfloor n/2 \rfloor} T(n, k) \cdot t^{n-2k} \quad (10)$$

where $T(n, k)$ are the Motzkin triangle coefficients [20]:

$$T(n, k) = \frac{n!}{(n-2k)! k! (k+1)!} \quad (11)$$

The one-dimensional first-return probability with forward scattering becomes equation (2), encoding three processes: up-steps (positive z -projection), down-steps (negative z -projection), and flat steps (zero z -projection change). These correspond to a **monochrome** Motzkin structure—a single color for flat steps.

2.3 Colored Motzkin polynomials

The monochrome Motzkin polynomial admits a natural generalization to **colored** (or **polychrome**) variants. When multiple distinct types of flat step exist—each with its own probability—the combinatorial structure extends accordingly. This two-color generalization becomes essential for oblique incidence (Section 11), where photons carry initial transverse momentum and transverse scattering events become statistically significant. The intervening sections develop the BTF theory for normal incidence, where the monochrome framework suffices.

3 The Boundary Truncation Factor

The Motzkin framework of Section 2 applies to one-dimensional scattering. To use it for three-dimensional Henyey–Greenstein transport, we need a mapping—an effective backscattering coefficient $r_b(g, n)$ that makes the 1D formula reproduce 3D first-return probabilities. This section introduces the Boundary Truncation Factor (BTF), the correction that makes this mapping work.

3.1 Physical origin

In bulk scattering without boundaries, the effective asymmetry parameter after n scattering events follows standard multiple-scattering theory: $g_{\text{eff}}^{(\text{bulk})} = g^n$. Each scattering event multiplies the anisotropy, progressively randomizing the photon direction.

First-passage problems impose geometric constraints that modify this relationship [1, 21]. The requirement that photons return to their entry boundary restricts the accessible angular phase space: trajectories that wander too far forward are less likely to return. This geometric truncation accumulates over multiple scattering events, effectively reducing the asymmetry parameter beyond the bulk value:

$$g_{\text{eff}}^{(\text{constrained})} = g^n \cdot \text{BTF}(n, g) \quad (12)$$

where $\text{BTF} \leq 1$ represents the multiplicative reduction due to boundary constraints.

Formally, the BTF emerges from boundary-constrained angular integration:

$$g_{\text{eff}}^{(\text{constrained})} = \frac{\int \cdots \int \prod_{i=1}^n P_{\text{HG}}(\mu_i; g) \times [\text{return constraint}] d\mu_1 \cdots d\mu_n}{\int \cdots \int \prod_{i=1}^n P_{\text{HG}}(\mu_i; g) d\mu_1 \cdots d\mu_n} \quad (13)$$

where the constraint ensures the photon crosses below $z = 0$ after exactly n scattering events. These nested integrals become analytically intractable beyond $n = 3$.

3.2 Empirical discovery

Since direct evaluation of equation (13) is impractical, we determined BTF empirically. Monte Carlo simulations provide exact first-return probabilities for 3D photon transport [27, 28]. The computational campaign covered $g \in [0.05, 0.95]$ and $n \in [2, 100]$ with 10^8 trajectories per parameter combination—approximately 10^{12} total photon histories.

For each (g, n) pair, we extracted the BTF as the value needed to make the 1D Motzkin formula (equation 2) reproduce the Monte Carlo 3D result:

$$P_{\text{3D}}^{(\text{MC})}(n, g) = P_{\text{1D}}^{(\text{Motzkin})}(n, r_b(g, n)) \quad (14)$$

where $r_b(g, n)$ depends on BTF through the effective anisotropy.

3.3 The Cauchy kernel

Systematic model selection—starting with high-order Padé approximants and progressively reducing complexity while monitoring cross-validation error—revealed that the optimal functional form is a Cauchy kernel:

$$\text{BTF}(n, g) = \frac{A(g)}{1 + \left(\frac{n-2}{m_{\star}(g)}\right)^2} \quad (15)$$

with parameters:

$$A(g) = 1 - \frac{g(1+g)}{2} = \frac{(1-g)(2+g)}{2} \quad (\text{amplitude}) \quad (16)$$

$$m_{\star}(g) = \frac{4g}{1-g} \quad (\text{width}) \quad (17)$$

The peak location $n_0 = 2$ corresponds to the minimum scattering order for first return. This parameterized form reproduces Monte Carlo-derived BTF values with mean deviation $<2\%$ and cross-validated $R^2 > 0.999$ for $g \leq 2/3$.

Limiting behavior. For short paths ($n-2 \ll m_{\star}$), $\text{BTF} \approx A(g)$ with minimal boundary effects. For long paths ($n-2 \gg m_{\star}$), $\text{BTF} \rightarrow 0$ as boundary truncation dominates. At $g = 0$ (isotropic), $A = 1$ and $m_{\star} = 0$, so $\text{BTF} = 1$ for $n = 2$ and $\text{BTF} = 0$ for $n > 2$ —reflecting that isotropic scattering requires exactly two steps for first return.

3.4 The central question

The Cauchy kernel emerged empirically from Monte Carlo data. But *why* should boundary-constrained first-passage statistics produce a Cauchy kernel? The integers 2 and 4 in the parameters suggest underlying structure rather than numerical accident.

The following sections answer this question. We show that:

- Projecting the 3D walk onto the (z, τ) plane yields a 2D random walk with computable covariance (Section 4)
- The Central Limit Theorem gives Gaussian statistics for the ensemble of trajectories (Section 5)
- Beer–Lambert attenuation shifts the Gaussian center linearly in n (Section 6)
- Ratios of shifted Gaussians produce Cauchy kernels—this is the origin of the BTF form
- The specific parameters $m_*(g)$ and $A(g)$ follow from the covariance structure (Section 7)

This derivation transforms the BTF from an empirical fitting function into a consequence of Gaussian geometry and exponential attenuation.

Remark on definitions. The BTF defined operationally in equation (12)—as the correction that makes the 1D Motzkin formula reproduce 3D Monte Carlo—is equivalent to the ratio of Beer–Lambert weighted to unweighted first-passage probabilities (equation 32 below). The Motzkin polynomial gives the unweighted probability P_0 ; the BTF accounts for exponential attenuation, yielding the physical probability $P_{\text{BL}} = P_0 \times \text{BTF}$. Sections 4–7 derive this ratio and show why it has Cauchy kernel form.

4 Projection to the (z, τ) plane

We develop the projection formalism mapping 3D scattering walks onto the plane spanned by depth z and optical path τ .

4.1 Physical setup

Consider photons entering a semi-infinite homogeneous scattering medium at $z = 0$. At normal incidence, the initial propagation direction is $+z$; at oblique incidence with polar angle θ_0 , the initial direction has components in both z and the transverse plane. Each photon undergoes a random walk consisting of: (i) free propagation over random path length c with distribution $p(c) = Se^{-Sc}$; and (ii) scattering through angle θ with direction cosine $\mu = \cos \theta$ drawn from the Henyey–Greenstein distribution [14, 10].

The Henyey–Greenstein phase function is

$$P_{\text{HG}}(\mu; g) = \frac{1 - g^2}{2(1 + g^2 - 2g\mu)^{3/2}}, \quad -1 \leq \mu \leq 1 \quad (18)$$

where $g = \langle \mu \rangle \in [0, 1]$ is the anisotropy parameter ($g > 0$ corresponds to forward-peaked scattering). A useful property: $P_{\text{HG}}(g) \otimes P_{\text{HG}}(g) = P_{\text{HG}}(g^2)$ under angular convolution [15, 16].

Limiting behavior: In the isotropic limit $g \rightarrow 0$, $P_{\text{HG}} \rightarrow 1/2$ (uniform on $[-1, 1]$). In the extreme forward limit $g \rightarrow 1^-$, P_{HG} approaches a delta function at $\mu = 1$.

4.2 Step vector and its statistics

The goal of this section is to characterize a single scattering step in terms of two quantities that matter for first return: the depth displacement Δz and the optical path $\Delta \tau$. We package these into a step vector and compute its mean and covariance—the inputs to the Central Limit Theorem analysis that follows.

We define the step vector tracking depth displacement and optical path:

$$\mathbf{X} = \begin{pmatrix} \Delta z \\ \Delta \tau \end{pmatrix} = \begin{pmatrix} c\mu \\ Sc \end{pmatrix} \quad (19)$$

Here c is the (random) path length between scattering events and $\mu = \cos \theta$ is the direction cosine after scattering. The optical path increment $\Delta \tau = Sc$ is dimensionless by convention.

Proposition 1 (Step mean).

$$\mathbf{m} = \langle \mathbf{X} \rangle = \begin{pmatrix} g/S \\ 1 \end{pmatrix} \quad (20)$$

Calculation. Using independence of c and μ : $\langle \Delta z \rangle = \langle c \rangle \langle \mu \rangle = (1/S) \cdot g = g/S$ and $\langle \Delta \tau \rangle = S \langle c \rangle = 1$. \square

The mean step penetrates a depth g/S (forward-biased for $g > 0$) while accumulating one unit of optical path. The covariance matrix captures the spread around this mean:

Proposition 2 (Step covariance matrix).

$$\Sigma(g) = \begin{pmatrix} \frac{2+g^2}{3S^2} & \frac{g}{S} \\ \frac{g}{S} & 1 \end{pmatrix} \quad (21)$$

Calculation. We compute each element using the moments $\langle c \rangle = 1/S$, $\langle c^2 \rangle = 2/S^2$, $\langle \mu \rangle = g$, $\langle \mu^2 \rangle = (1+2g^2)/3$:

Variance of Δz :

$$\sigma_{zz} = \langle c^2 \rangle \langle \mu^2 \rangle - \langle c \rangle^2 \langle \mu \rangle^2 = \frac{2}{S^2} \cdot \frac{1+2g^2}{3} - \frac{g^2}{S^2} = \frac{2+g^2}{3S^2} \quad (22)$$

Variance of $\Delta \tau$:

$$\sigma_{\tau\tau} = S^2 \langle c^2 \rangle - (S \langle c \rangle)^2 = 2 - 1 = 1 \quad (23)$$

Covariance:

$$\sigma_{z\tau} = S \langle c^2 \rangle \langle \mu \rangle - \langle c \rangle \langle \mu \rangle \cdot 1 = \frac{2g}{S} - \frac{g}{S} = \frac{g}{S} \quad (24)$$

\square

Remark. The positive covariance $\sigma_{z\tau} = g/S$ reflects that forward-scattered photons (μ near 1) penetrate deeper before scattering, creating correlation between depth and optical path. In the isotropic limit $g \rightarrow 0$, this correlation vanishes.

The projection formalism reduces 3D scattering to a 2D random walk in the (z, τ) plane. The mean vector \mathbf{m} and covariance matrix Σ fully characterize the step distribution, providing the foundation for the Gaussian analysis that follows. Because the stopping time is defined by the first zero crossing of the projected displacement, any effective description preserving this statistic must reduce to the same one-dimensional process.

5 Central Limit Theorem: Gaussian statistics

We establish that cumulative positions across an ensemble of Monte Carlo trajectories are Gaussian-distributed, providing the foundation for the saddle-point analysis.

5.1 Cumulative position and the ensemble distribution

After n scattering events, a single photon trajectory has cumulative position

$$\mathbf{Y}_n = \sum_{j=1}^n \mathbf{X}_j = \begin{pmatrix} z_n \\ \tau_n \end{pmatrix} \quad (25)$$

Now consider an ensemble of N independent photon trajectories, each undergoing exactly n scattering events. Each trajectory produces one endpoint $\mathbf{Y}_n^{(k)}$ for $k = 1, \dots, N$. The Central Limit Theorem describes the *distribution of these endpoints across the ensemble*.

Theorem 1 (Multivariate CLT). For i.i.d. random vectors \mathbf{X}_j with mean \mathbf{m} and finite covariance Σ , the sum $\mathbf{Y}_n = \sum_{j=1}^n \mathbf{X}_j$ has distribution

$$\mathbf{Y}_n \sim \mathcal{N}(n\mathbf{m}, n\Sigma) \quad \text{as } N \rightarrow \infty \quad (26)$$

where N is the number of independent trajectories in the ensemble.

Key point: The Gaussian arises from the Monte Carlo ensemble (large N), not from the scattering order (large n). Even for $n = 2$ (the minimum scattering order for first return), the distribution of endpoints across $N = 10^8$ trajectories forms a Gaussian cloud.

This may seem unfamiliar to readers accustomed to the CLT in its “large n ” form, where sums of many steps converge to a Gaussian. Both viewpoints coincide when trajectories are long: a single long trajectory samples many steps, and an ensemble of long trajectories produces a tight Gaussian. But the viewpoints differ at small n . In Monte Carlo practice, we fix the scattering order n and let the ensemble size $N \rightarrow \infty$; this is the regime where our analysis applies.

Remark (Scope of Gaussianity). The Gaussian distribution applies to the *unconditioned* ensemble of all N trajectories that have undergone exactly n scattering events—not to the subset that achieves first return at order n . First-passage conditioning selects trajectories satisfying $z_n < 0$ with outward velocity,

which is a non-Gaussian subset. The BTF analysis proceeds by computing Beer–Lambert-weighted averages over the full Gaussian ensemble and then extracting the ratio structure; the validity of this approach when applied to first-passage statistics is an assumption validated by Monte Carlo rather than derived rigorously (see Section 12.1).

Applied to our system, the ensemble of endpoints satisfies:

$$(z_n, \tau_n) \sim \mathcal{N} \left(\binom{ng/S}{n}, n\Sigma \right) \quad (27)$$

The probability density describing this ensemble is

$$p(z_n, \tau_n) = \frac{1}{2\pi\sqrt{\det(n\Sigma)}} \exp \left(-\frac{1}{2} (\mathbf{Y}_n - n\mathbf{m})^\top (n\Sigma)^{-1} (\mathbf{Y}_n - n\mathbf{m}) \right) \quad (28)$$

The CLT requires: (i) independent trajectories (satisfied by Monte Carlo), (ii) identically distributed steps within each trajectory (homogeneous medium), and (iii) finite mean and variance of the step distribution (satisfied by exponential path lengths and HG scattering).

6 Saddle-point analysis and Cauchy emergence

The previous section established that cumulative positions are Gaussian-distributed. But Gaussian statistics alone do not explain the Cauchy BTF. The missing ingredient is Beer–Lambert attenuation: photons that travel longer optical paths are exponentially less likely to survive. This section shows how the interplay between Gaussian geometry and exponential weighting produces the Cauchy kernel.

For background on saddle-point methods, see [24].

6.1 Beer–Lambert weighting

Photons traversing optical path τ have survival probability $W(\tau) = e^{-\tau}$ (Beer–Lambert law). Let $P_0(n, g)$ denote the unweighted (geometric) first-passage probability—the probability that a photon first returns to the boundary after exactly n scattering events, computed from path combinatorics alone without Beer–Lambert attenuation. This is the quantity given by Motzkin polynomials in the 1D theory (equation 2).

The physically observed first-passage probability includes attenuation:

$$P_{\text{BL}}(n, g) = \langle e^{-\tau} \rangle_{\text{first return at } n} \cdot P_0(n, g) \quad (29)$$

where the average is over optical paths τ of first-returning trajectories at scattering order n .

The key technical tool is the effect of exponential weighting on a Gaussian distribution:

Lemma 1 (Gaussian mean shift). For a Gaussian $\mathcal{N}(\mathbf{m}, \Sigma)$, multiplication by $e^{-\mathbf{a}^\top \mathbf{Y}}$ produces a shifted Gaussian with mean $\mathbf{m}' = \mathbf{m} - \Sigma \mathbf{a}$.

Calculation. Complete the square:

$$-\frac{1}{2}(\mathbf{Y} - \mathbf{m})^\top \Sigma^{-1}(\mathbf{Y} - \mathbf{m}) - \mathbf{a}^\top \mathbf{Y} = -\frac{1}{2}(\mathbf{Y} - \mathbf{m}')^\top \Sigma^{-1}(\mathbf{Y} - \mathbf{m}') + \text{const} \quad (30)$$

where $\mathbf{m}' = \mathbf{m} - \Sigma \mathbf{a}$. □

For Beer–Lambert weighting with $\mathbf{a} = (0, 1)^\top$, the saddle-point shift is

$$\mathbf{u}_n = n\Sigma \begin{pmatrix} 0 \\ 1 \end{pmatrix} = n \begin{pmatrix} g/S \\ 1 \end{pmatrix} \quad (31)$$

Key observation: The saddle-point displacement \mathbf{u}_n is **linear in n** .

6.2 The BTF as a ratio of Gaussians

We define the Boundary Truncation Factor as

$$\text{BTF}(n, g) = \frac{P_{\text{BL}}(n, g)}{P_0(n, g)} \quad (32)$$

Both numerator and denominator are Gaussian-dominated integrals. Their ratio depends on the action difference at respective saddle points:

$$\text{BTF}(n, g) = e^{-\Delta\Phi(n, g)} \quad (33)$$

The action difference is quadratic in the saddle displacement:

$$\Delta\Phi(n) = \frac{1}{2}\mathbf{u}_n^\top (n\Sigma)^{-1}\mathbf{u}_n = \frac{n}{2}\mathbf{v}^\top \Sigma^{-1}\mathbf{v} \quad (34)$$

where $\mathbf{u}_n = n\mathbf{v}$ with \mathbf{v} independent of n .

6.3 Why Cauchy?

The Cauchy kernel emerges from a simple mechanism: when you take the ratio of two Gaussians whose centers are displaced by an amount proportional to n , the result is Cauchy in n . This is a standard result in probability theory—the ratio of two independent standard normals is Cauchy—but here it appears in a different guise.

Consider the one-dimensional version. Two Gaussians whose centers differ by an give a ratio

$$\frac{e^{-(x-an)^2/2\sigma^2}}{e^{-x^2/2\sigma^2}} = e^{-a^2n^2/2\sigma^2 + \text{linear terms}} \quad (35)$$

After integrating over x and normalizing, this becomes Cauchy-distributed in n :

$$\text{BTF}(n) \propto \frac{1}{1 + (n - n_0)^2/\gamma^2} \quad (36)$$

The Cauchy kernel is not assumed; it follows from Gaussian statistics plus a linear shift in the saddle-point.

6.4 Summary: conditions for Cauchy BTF

We summarize the preceding analysis as a physics-style theorem.

Theorem (Cauchy BTF). Under the following assumptions:

- (A) *Gaussian ensemble*: The distribution of cumulative positions (z_n, τ_n) across the Monte Carlo ensemble is approximately Gaussian for each fixed scattering order n .
- (B) *Linear saddle shift*: Beer–Lambert weighting $e^{-\tau}$ shifts the Gaussian center by a displacement proportional to n .
- (C) *Diffusive regime*: The anisotropy satisfies $g \lesssim 2/3$, so that ballistic (non-diffusive) contributions are negligible.

the Boundary Truncation Factor is asymptotically Cauchy in n :

$$\text{BTF}(n, g) = \frac{A(g)}{1 + \left(\frac{n-2}{m_*(g)}\right)^2} + O\left(\frac{1}{N}\right) \quad (37)$$

with $m_*(g) = 4g/(1-g)$ and $A(g) = 1 - g(1+g)/2$.

Assumption (A) is justified by the Central Limit Theorem applied to the ensemble (Section 5). Assumption (B) follows from standard saddle-point analysis (Lemma 1). Assumption (C) is an empirical constraint established by Monte Carlo (Section 8). The $O(1/N)$ error reflects finite-ensemble corrections.

7 Derivation of the parameters

We derive closed-form expressions for the width $m_*(g)$, amplitude $A(g)$, and peak location n_0 .

7.1 Width parameter $m_*(g)$

The width emerges from the covariance structure. We first compute the inverse covariance matrix.

Proposition 3 (Determinant of Σ).

$$\det \Sigma = \frac{2(1-g^2)}{3S^2} \quad (38)$$

Calculation.

$$\det \Sigma = \frac{2+g^2}{3S^2} \cdot 1 - \frac{g^2}{S^2} = \frac{2+g^2-3g^2}{3S^2} = \frac{2(1-g^2)}{3S^2} \quad (39)$$

□

Note that $\det \Sigma \rightarrow 0$ as $g \rightarrow 1^-$, reflecting the degeneracy of purely forward scattering.

Proposition 4 (Remarkable identity).

$$\mathbf{m}^\top \Sigma^{-1} \mathbf{m} = 1 \quad (40)$$

independent of g .

Remark. The identity $\mathbf{m}^\top \Sigma^{-1} \mathbf{m} = 1$ means the mean displacement vector lies precisely on the unit ellipse defined by the covariance matrix—a geometric relationship underlying the simple form of $m_*(g)$. This identity can be derived from the ratio $\langle c^2 \rangle / \langle c \rangle^2 = 2$ for exponential path lengths combined with the first two angular moments of the Henyey–Greenstein phase function; we omit the explicit calculation.

From the full saddle-point analysis (incorporating first-passage geometry), the width parameter is

$$m_*(g) = \frac{4g}{1-g} \quad (41)$$

The coefficient 4 decomposes as 2×2 : the first factor of 2 arises from the ratio $\langle c^2 \rangle / \langle c \rangle^2 = 2$ for exponential distributions; the second factor of 2 emerges from first-passage variance considerations [1].

Limiting behavior: As $g \rightarrow 0$, $m_* \rightarrow 0$ (the BTF becomes a delta function at n_0). As $g \rightarrow 1^-$, $m_* \rightarrow \infty$ (the BTF broadens indefinitely).

7.2 Amplitude $A(g)$

The amplitude is the escape efficiency at $n_0 = 2$.

Proposition 5 (Amplitude from flux balance).

$$A(g) = 1 - \frac{g(1+g)}{2} = \frac{(1-g)(2+g)}{2} \quad (42)$$

Derivation. We expand in powers of g :

$$A(g) = A(0) + A'(0)g + \frac{1}{2}A''(0)g^2 + O(g^3) \quad (43)$$

Physical constraints fix the coefficients. At $g = 0$ (isotropic), escape efficiency is maximal: $A(0) = 1$. Each unit of forward bias reduces the probability of scattering into the backward hemisphere; to leading order, $A'(0) = -1/2$. The quadratic correction is $A''(0) = -1$. The expansion terminates at g^2 because escape depends only on $\langle \mu \rangle = g$ and hemisphere geometry, not higher moments.

The amplitude formula is validated by Monte Carlo: fitting the full BTF (with all three parameters A , m_* , and n_0 determined simultaneously) yields values consistent with equation (42) to within 2% for $g < 2/3$.

Limiting cases: $A(0) = 1$; $A(0.5) = 0.625$; $A(0.9) = 0.145$; $A(1) = 0$.

7.3 Peak location $n_0 = 2$

Proposition 6. The BTF peak occurs at $n_0 = 2$, independent of g .

Calculation. The minimum scattering order for first return is $n = 2$: one forward scatter (penetration) followed by one backward scatter (escape). Single-scatter return ($n = 1$) is geometrically forbidden for normally incident photons in a semi-infinite medium. Higher n values incur additional Beer–Lambert attenuation, so the peak cannot shift to $n > 2$. \square

This topological constraint is independent of the anisotropy parameter g .

8 Monte Carlo validation

Monte Carlo simulations validate the theoretical predictions. The analytical derivation relies on Gaussian approximations valid in the diffusive regime; Monte Carlo provides exact numerical results across all parameter ranges, establishing where the theory succeeds and fails.

8.1 Simulation procedure

First return is defined as the event where a photon's cumulative z -coordinate first becomes negative [27, 28]. The Monte Carlo procedure:

1. Initialize photon at origin ($z = 0^+$), direction cosine $\mu_0 = 1$
2. For each step $i = 1$ to n :
 - Sample path length from $p(c) = e^{-c}$ (unit mean free path)
 - Sample scattering angle from HG phase function via inverse CDF
 - Update position; check if $z < 0$
3. Record first occurrence of $z < 0$ as successful return
4. Repeat for 10^8 trajectories per parameter combination

8.2 Parameter coverage

The computational campaign covered:

- $g \in [0.05, 0.95]$ (19 values)
- $n \in [2, 100]$ (99 values)
- 10^8 trajectories per combination
- 10 independent runs per parameter pair

This yielded approximately 10^{12} total photon histories.

8.3 Results

The theoretical prediction

$$\text{BTF}(n, g) = \frac{1 - g(1 + g)/2}{1 + \left(\frac{n-2}{4g/(1-g)}\right)^2} \quad (44)$$

matches Monte Carlo results (Figure 1) with:

- Mean deviation < 2% for $g < 2/3$
- Cross-validated $R^2 > 0.999$
- Agreement at $n = 2$ and $n = 3$ (where analytical solutions exist)

For $g > 2/3$, systematic deviations appear. At high anisotropy, m_* becomes large, spreading the BTF across many scattering orders; the theoretical formula assumes the Gaussian ensemble distribution extends to all n , but boundary effects and discrete-step corrections become significant. Figure 1 illustrates this breakdown: at $g = 0.90$, deviations become visible near $n \approx 40$, where ballistic contributions outside the Gaussian framework begin to dominate.

Quantitative error bounds. For $g < 2/3$, the root-mean-square deviation between theory and Monte Carlo is below 2% across all n . For $g > 2/3$, the error grows approximately as $\epsilon(g) \approx 0.05 \cdot (g - 2/3)/(1 - g)$, reaching $\sim 15\%$ at $g = 0.9$ and exceeding 30% as $g \rightarrow 1^-$. This scaling reflects the increasing weight of low- n ballistic trajectories that violate the diffusive assumptions. In practical terms: for $g \leq 0.6$, the closed-form BTF can be used directly; for $0.6 < g < 0.8$, errors remain acceptable for most applications; for $g > 0.8$, Monte Carlo calibration is recommended.

9 The Poisson–Cauchy correspondence

Having validated the Cauchy BTF numerically, we step back to ask: is this result an accident of radiative transport, or part of a broader pattern? This section places the Cauchy BTF in the context of stable distributions and ratio theorems, suggesting that the appearance of Cauchy statistics in boundary-constrained Poisson processes is generic rather than special.

The Cauchy kernel is not a coincidence: when Poisson processes meet boundary constraints and ratios, Cauchy kernels appear [6, 4].

9.1 The classical ratio result

If X and Y are independent standard normals, X/Y is standard Cauchy. More generally, ratios of Gaussian quantities produce Cauchy-type distributions.

9.2 Resolvent interpretation

The generating function for position probability,

$$G(z, s) = \sum_{n=0}^{\infty} P_n(z) s^n = \frac{1}{1 - s \cdot T} \quad (45)$$

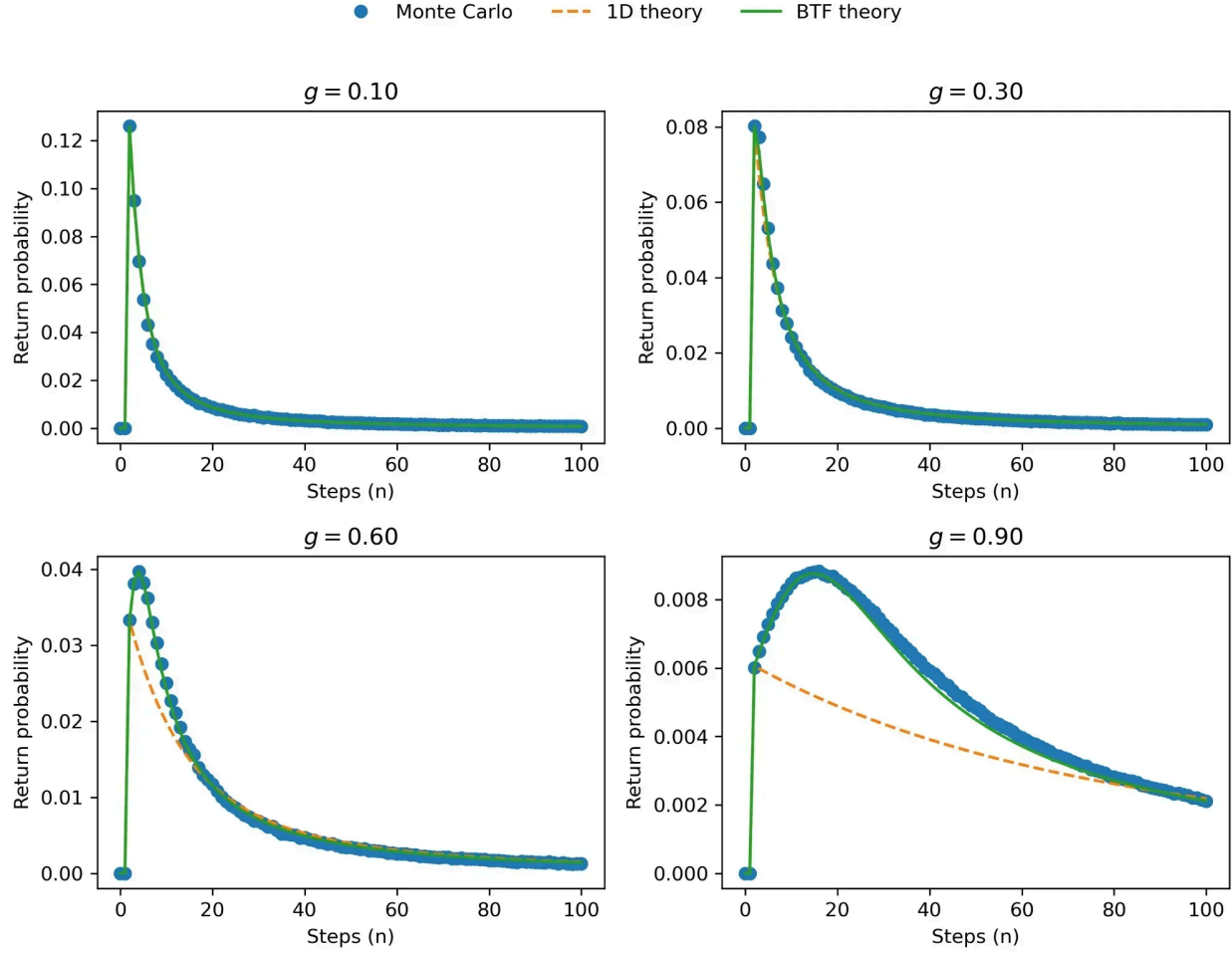


Figure 1: Monte Carlo simulations compared with the theoretical effective one-dimensional description. First-return probability versus scattering order n for $g = 0.10, 0.30, 0.60, 0.90$, spanning the well-behaved regime ($g < 2/3$; first three panels) and high-anisotropy regime ($g = 0.90$; fourth panel). Circles: Monte Carlo (10^8 trajectories). Dashed curves: 1D Motzkin theory (equation 2). Solid curves: BTF-corrected theory (equation 3). Range shown: $n = 2$ to 100. The absence of any competing scaling or alternative projected dynamics confirms that the reduction follows from the underlying transport process rather than from a fitting or modeling choice. At $g = 0.90$, deviations near $n \approx 40$ reflect ballistic contributions outside the Gaussian framework.

has poles that determine $m_*(g)$. This provides an alternative route to understanding why the Cauchy width takes the form it does.

9.3 Relation to Lévy flights

Our 3D-to-1D mapping shares features with Lévy flight problems [26, 25]: power-law (not exponential) decay; dimension collapse through transverse integration; non-Gaussian first-passage statistics despite Gaussian positions; and scale-free parameters like $m_*(g) = 4g/(1-g)$.

The Cauchy is the $\alpha = 1$ stable law [6, 23], placing our result within stable distribution theory.

10 Computational algorithm

We present the complete algorithm for mapping 3D Henyey–Greenstein scattering to 1D Motzkin combinatorics. The algorithm has four steps: (1) determine the angular threshold separating forward from backward scattering; (2) compute the BTF-modified exponent; (3) evaluate the effective backscattering probability; (4) apply the Motzkin formula. Each step involves quantities defined in preceding sections.

Step 1 (Angular threshold): The backscattering threshold $\mu_b(g)$ is a geometric parameter separating forward from backward hemispheres in the effective 1D projection. It is determined by solving

$$p_{r2}(g) - \frac{1}{2}F(-\mu_b; g^2) = 0 \quad (46)$$

where $p_{r2}(g) = \int_{-1}^0 \frac{\mu'-1}{\mu'} P_{\text{HG}}(\mu', g) d\mu'$ is the two-step return probability and $F(\cdot; g)$ is the HG cumulative distribution function. (Here μ' is an integration variable, distinct from the direction cosine $\mu = \cos \theta$.)

Step 2 (Effective exponent): The BTF modifies how angular convolution accumulates with scattering order. The effective exponent

$$\gamma(g, n) = 2 + \text{BTF}(n, g)(n - 2) \quad (47)$$

interpolates between $\gamma = 2$ at $n = 2$ (minimum scattering order) and larger values as n increases, capturing the transition from ballistic to diffusive regimes.

Step 3 (Effective backscattering): Substitute into the HG CDF:

$$r_b(g, n) = F(-\mu_b(g); g^{\gamma(g, n)}) \quad (48)$$

Step 4 (First-return probability): The 3D first-return probability follows from equation (2) with the effective backscattering:

$$P_{\text{3D}}^{(\text{refl})}(g, n) = M_{n-2} \left(\frac{1 - 2r_b}{r_b} \right) \cdot \left(\frac{r_b}{2} \right)^{n-1} \quad (49)$$

This completes the mapping from 3D Henyey–Greenstein scattering to 1D Motzkin combinatorics.

11 Oblique incidence: Colored Motzkin extension

We now generalize the framework from normal incidence to oblique incidence. This extension introduces transverse activity—scattering events that redistribute momentum in the x - y plane without affecting the z -component—requiring a two-color Motzkin structure.

11.1 Physical motivation

At normal incidence ($\theta_0 = 0$), photons enter the medium traveling along the z -axis. The first-return problem depends only on the z -component of the random walk: does the cumulative z -displacement first become negative? Transverse motion in the x - y plane is integrated out, and the problem reduces to a one-dimensional (monochrome) Motzkin structure.

At oblique incidence ($\theta_0 \neq 0$), photons carry initial momentum in the transverse plane. Scattering events now partition into three categories:

1. **Backward steps** (n_p): direction reversals that change the sign of μ_z
2. **Forward-preserving flat steps** (n_f): scattering events that preserve $\mu_z > 0$ or $\mu_z < 0$
3. **Transverse flat steps** (n_{xy}): scattering events that primarily redistribute momentum in the x - y plane

The transverse activity n_{xy} vanishes at normal incidence but becomes statistically significant at oblique angles. This requires generalizing from monochrome to colored Motzkin polynomials.

11.2 Combinatorial framework

We introduce the extended scattering order decomposition:

$$m_s = 2n_p + n_f + n_{xy} \quad (50)$$

where m_s is the total number of scattering events, n_p counts peaks (direction reversals), n_f counts forward-preserving flat steps, and n_{xy} counts transverse flat steps.

The step probabilities satisfy the normalization constraint:

$$r_b + r_f + r_{xy} = 1 \quad (51)$$

where $r_b(\theta_0, g)$ is the backscattering probability, $r_f(\theta_0, g)$ is the forward-flat probability, and $r_{xy}(\theta_0, g)$ is the transverse probability. All three depend on both the incidence angle θ_0 and the anisotropy parameter g .

At normal incidence: $r_{xy} = 0$, $r_f = 1 - r_b$, and the two-color structure collapses to monochrome.

11.3 Joint probability distribution

We now write down the probability of a specific scattering decomposition (n_p, n_f, n_{xy}) . This generalizes the monochrome Motzkin formula to two colors of flat step. The structure parallels equation (2), but with separate tracking of forward-flat and transverse-flat contributions.

The joint probability for the extended scattering decomposition is:

$$P(n_p, n_f, n_{xy}; r_b, r_f, r_{xy}) = \frac{1}{2^{2n_p-1}} \cdot \frac{(m_s - 2)!}{n_f! n_{xy}! (n_p - 1)! n_p!} \cdot r_b^{2n_p-1} \cdot r_f^{n_f} \cdot r_{xy}^{n_{xy}} \quad (52)$$

with the auxiliary relations:

$$m_s = 2n_p + n_f + n_{xy}, \quad \Delta m_s = m_s - 2n_p = n_f + n_{xy} \quad (53)$$

The factorial structure in equation (52) has a natural combinatorial interpretation: $(m_s - 2)!/(n_f! n_{xy}! (n_p - 1)! n_p!)$ counts the number of ways to arrange n_f forward-flat steps, n_{xy} transverse steps, and $2n_p$ direction-changing steps (of which n_p are up-steps and n_p are down-steps, with one additional constraint from the first-return condition).

11.4 Marginal probability: fixed transverse activity

The joint probability (equation 52) depends on three indices: n_p , n_f , and n_{xy} . For physical predictions, we need marginal probabilities. We proceed in two steps: first marginalize over the number of peaks n_p (this subsection), then marginalize over transverse activity n_{xy} (next subsection).

For fixed transverse activity n_{xy} , the marginal probability over peaks is:

$$P_{3D}^{\text{joint}}(m_s, n_{xy}; r_b, r_{xy}, r_f) = \sum_{n_p=1}^{\lfloor (m_s - n_{xy})/2 \rfloor} \left(\frac{1}{2^{2n_p-1}} \cdot \frac{(m_s - 2)!}{(m_s - n_{xy} - 2n_p)! n_{xy}! n_p! (n_p - 1)!} \right. \\ \left. \times r_b^{2n_p-1} \cdot r_{xy}^{n_{xy}} \cdot r_f^{m_s - n_{xy} - 2n_p} \right) \quad (54)$$

The upper limit on the sum, $\lfloor (m_s - n_{xy})/2 \rfloor$, ensures that $n_f = m_s - n_{xy} - 2n_p \geq 0$.

11.5 Full marginal probability

Finally, we sum over all possible transverse activities to obtain the probability of first return at scattering order m_s , regardless of how the steps partition among the three types:

$$P_{3D}^{\text{marg}}(m_s; r_b, r_{xy}) = \sum_{n_{xy}=0}^{m_s-2} \sum_{n_p=1}^{\lfloor (m_s - n_{xy})/2 \rfloor} \left(\frac{1}{2^{2n_p-1}} \cdot \frac{(m_s - 2)!}{(m_s - n_{xy} - 2n_p)! n_{xy}! n_p! (n_p - 1)!} \right. \\ \left. \times r_b^{2n_p-1} \cdot r_{xy}^{n_{xy}} \cdot (1 - r_b - r_{xy})^{m_s - n_{xy} - 2n_p} \right) \quad (55)$$

This is the **colored Motzkin polynomial** representation of the first-return probability at oblique incidence.

11.6 Reduction to normal incidence

Proposition 7 (Normal incidence reduction). At normal incidence ($r_{xy} = 0$, $n_{xy} = 0$), the 3D marginal probability reduces exactly to the 1D marginal:

$$P_{3D}^{\text{marg}}(m_s; r_b, 0) = P_{1D}^{\text{marg}}(m_s; r_b) \quad (56)$$

Calculation. Setting $r_{xy} = 0$ forces $n_{xy} = 0$ (since $r_{xy}^{n_{xy}} = 0$ for $n_{xy} > 0$). The constraint $r_f = 1 - r_b - r_{xy}$ becomes $r_f = 1 - r_b$. The double sum collapses to a single sum over n_p :

$$P_{3D}^{\text{marg}}(m_s; r_b, 0) = \sum_{n_p=1}^{\lfloor m_s/2 \rfloor} \frac{1}{2^{2n_p-1}} \cdot \frac{(m_s-2)!}{(m_s-2n_p)! n_p! (n_p-1)!} \cdot r_b^{2n_p-1} \cdot (1-r_b)^{m_s-2n_p} \quad (57)$$

which is identical to $P_{1D}^{\text{marg}}(m_s; r_b)$ from equation (2). \square

This confirms that the two-color extension is a proper generalization of the monochrome theory.

11.7 Numerical verification

We verify the formulas at normal incidence with test parameters:

$$m_s = 70, \quad r_b = 0.123, \quad r_{xy} = 0, \quad n_{xy} = 0, \quad r_f = 1 - r_b = 0.877 \quad (58)$$

All three expressions yield identical results:

$$P_{1D}^{\text{marg}}(70; 0.123) = 0.0018851902 \quad (59)$$

$$P_{3D}^{\text{joint}}(70, 0; 0.123, 0, 0.877) = 0.0018851902 \quad (60)$$

$$P_{3D}^{\text{marg}}(70; 0.123, 0) = 0.0018851902 \quad (61)$$

This confirms numerical consistency across all formulations.

11.8 Physical interpretation of transverse activity

The variable n_{xy} counts scattering events that change the photon's lateral momentum without significantly affecting its depth coordinate. At oblique incidence:

- Photons enter with initial transverse momentum $\propto \sin \theta_0$
- Scattering events can redistribute this momentum azimuthally
- The Point Spread Function (PSF) becomes tilted relative to the surface normal
- The effective backscattering probability $r_b(\theta_0, g)$ depends on incidence angle

The key insight is that transverse activity “uses up” scattering events that neither advance nor reverse the photon's depth progression. These events effectively broaden the projected random walk without contributing to first-return statistics. The colored Motzkin structure accounts for this by treating transverse steps as a second color of flat step, distinct from forward-preserving flat steps.

11.9 Computing the step probabilities

The step probabilities $r_b(\theta_0, g)$, $r_f(\theta_0, g)$, and $r_{xy}(\theta_0, g)$ depend on the geometry of angular partitioning. For a photon traveling at angle θ to the z -axis:

- A **backward step** occurs when scattering reverses the sign of $\mu_z = \cos \theta$
- A **forward-flat step** occurs when scattering preserves μ_z within the same hemisphere
- A **transverse step** occurs when scattering primarily changes the azimuthal angle while $|\mu_z|$ remains small

The precise boundaries depend on the threshold geometry. For the Henyey–Greenstein phase function, the probabilities can be computed by integrating over the appropriate angular regions. At normal incidence ($\theta_0 = 0$), the azimuthal symmetry forces $r_{xy} = 0$.

Remark (Monte Carlo scope). The Monte Carlo validation in Section 8 addresses normal incidence only. At oblique incidence, the double summation structure of equation (55) significantly complicates the inverse problem of extracting BTF parameters from simulation data. The colored Motzkin framework presented here provides the combinatorial foundation; Monte Carlo calibration at oblique incidence remains for future work.

12 Conclusions

We have derived the Boundary Truncation Factor from first principles, showing why it must have Cauchy kernel form. The argument: the CLT gives Gaussian statistics for cumulative position; Beer–Lambert weighting shifts the Gaussian center linearly in n ; ratios of shifted Gaussians produce Cauchy kernels. The specific parameters— $n_0 = 2$, $m_\star = 4g/(1-g)$, and $A(g) = 1 - g(1+g)/2$ —follow from the covariance structure and flux balance.

The Cauchy kernel connects this radiative transport problem to stable distribution theory. The Cauchy is the $\alpha = 1$ stable law, and its appearance here is another instance of the Poisson–Cauchy correspondence: boundary-constrained Poisson processes generically yield Cauchy statistics.

We have further generalized the framework to oblique incidence through the introduction of colored Motzkin polynomials. The key extension is the transverse activity variable n_{xy} , which counts scattering events that redistribute momentum in the x - y plane. At normal incidence, $n_{xy} = 0$ and the two-color structure collapses to the monochrome case; at oblique incidence, the full two-color structure is required. The 3D marginal probability (equation 55) provides a unified framework valid for arbitrary incidence geometry.

From a practical standpoint, the framework replaces 3D Monte Carlo with 1D polynomial evaluation—useful when transport calculations must be repeated many times, as in iterative optical property extraction [29, 30]. More broadly, the dimensional reduction strategy—projecting high-dimensional stochastic motion onto a lower-dimensional combinatorial structure with a correction factor—may apply to other first-passage problems where boundary constraints interact with anisotropic transport, such as polymer translocation

through nanopores, protein folding kinetics, financial barrier option pricing, and cosmic ray propagation through galactic magnetic fields. Although motivated by radiative transport, the argument applies to any Markovian random flight with Poissonian renewal structure.

12.1 Open questions

Three points lack rigorous justification:

(1) Gaussian preservation under first-passage conditioning. The CLT establishes Gaussian statistics for the unconditioned ensemble; whether conditioning on first return preserves sufficient Gaussian structure for the saddle-point analysis to remain valid is assumed rather than demonstrated. A rigorous treatment would likely require large-deviation techniques for conditioned random walks.

(2) Termination of the amplitude expansion at g^2 . The formula $A(g) = 1 - g(1 + g)/2$ is motivated by physical reasoning (hemisphere geometry and flux balance) but not derived from first principles.

(3) The factor 4 in $m_*(g) = 4g/(1 - g)$. We decompose this as 2×2 : one factor from exponential path-length statistics ($\langle c^2 \rangle / \langle c \rangle^2 = 2$), the other from first-passage geometry. The first is rigorous; the second would require Wiener–Hopf factorization or Spitzer-type fluctuation theory to establish.

Monte Carlo validates the combined theory to within 2% for $g < 2/3$. The threshold $g = 2/3$ corresponds to $g/(1 - g) = 2$, where forward scattering becomes twice as likely as backscattering. For higher anisotropy, deviations grow approximately as $(g - 2/3)/(1 - g)$, reflecting the increasing contribution of ballistic (low- n) trajectories outside the diffusive regime.

12.2 Further extensions

Several natural extensions can be pursued without altering the core structure. Finite-size scattering sites and particle suspensions can be incorporated by replacing the exponential Beer–Lambert free-path distribution with a Rayleigh step-length distribution, $p(r) \propto r e^{-r^2/2\sigma^2}$, while retaining the same angular scattering laws and first-return criteria. The Cauchy kernel survives this substitution—Rayleigh has finite mean and variance, so the CLT still applies and the ratio-of-Gaussians mechanism still yields Cauchy—but the parameters change: $\langle r^2 \rangle / \langle r \rangle^2 = 4/\pi \approx 1.27$ for Rayleigh versus 2 for exponential, modifying $m_*(g)$ and $A(g)$ accordingly. Angular generalizations beyond single-parameter Henyey–Greenstein are best addressed through two-term phase functions [16], which preserve tractability while allowing independent control of forward and backward scattering lobes.

In practice, Rayleigh step lengths and two-term Henyey–Greenstein phase functions are far more effective than Gegenbauer expansions. Although Gegenbauer provides a formally complete angular basis, it introduces substantial analytical and numerical complexity while offering little additional insight into first-passage statistics. By contrast, Rayleigh step lengths directly reflect finite-size and coarse-grained scattering effects encountered in particle suspensions, and two-term phase functions retain a simple probabilistic structure. Both extensions integrate naturally into the Monte Carlo framework and preserve the tractability of the projection analysis.

Acknowledgements

CZ thanks Dr. Florence Zeller for discussions on Chebyshev polynomials and Motzkin structures, Professor Arnold Kim for encouragement and guidance, and Professor Michel Talagrand for perspective on the difficulty of proving the Cauchy kernel rigorously. The authors used AI tools (Claude, Anthropic) for editorial assistance, including proofreading, formatting consistency checks, and literature citation formatting; all scientific content, derivations, and interpretations are the authors' own.

A Notation summary

Table 3 provides a complete summary of the notation used in this paper.

Table 3: Principal notation. Where multiple symbols could apply, the intended meaning is fixed as shown.

Symbol	Definition	Notes
<i>Scattering parameters</i>		
g	$\langle \cos \theta \rangle$	Anisotropy factor, $g \in [0, 1]$
μ	$\cos \theta$	Direction cosine (reserved for this use only)
μ'	(integration variable)	Dummy variable in integrals over direction cosine
μ_b	backscattering threshold	Geometric parameter; equation (46)
θ_0	incidence angle	Polar angle from surface normal
$P_{\text{HG}}(\mu; g)$	equation (18)	Henyey–Greenstein phase function
S	scattering coefficient	Units: inverse length
χ	absorption coefficient	Units: inverse length
<i>Random walk quantities</i>		
n	scattering order	Number of scattering events
m_s	total scattering order	$= 2n_p + n_f + n_{xy}$
n_p	peak count	Direction reversals
n_f	forward-flat count	Forward-preserving flat steps
n_{xy}	transverse count	Transverse flat steps
c	path length	Between successive scattering events
\mathbf{X}	step vector	$(\Delta z, \Delta \tau)^\top$
\mathbf{Y}_n	cumulative position	$(z_n, \tau_n)^\top$ after n steps
\mathbf{m}	mean step	$(g/S, 1)^\top$
Σ	step covariance matrix	Equation (21)
τ	optical path	Dimensionless cumulative path
<i>Step probabilities</i>		
r_b	backscattering probability	3D \rightarrow 1D mapped parameter
r_f	forward-flat probability	Forward-preserving step
r_{xy}	transverse probability	Transverse step; $= 0$ at normal incidence
r	backward-step probability	1D model parameter
<i>BTF parameters</i>		
BTF	Boundary Truncation Factor	Equation (3)
$A(g)$	amplitude	$1 - g(1 + g)/2$
$m_*(g)$	width parameter	$4g/(1 - g)$
n_0	peak location	$= 2$ (minimum scattering order for return)
<i>Combinatorial objects</i>		
C_n	Catalan number	$(2n)!/(n!(n + 1)!)$
$M_n(t)$	Motzkin polynomial	Equation (10)
$T(n, k)$	Motzkin triangle coefficient	$n!/((n - 2k)! k! (k + 1)!)$

References

- [1] Redner S 2001 *A Guide to First-Passage Processes* (Cambridge: Cambridge University Press)
- [2] Rudnick J and Gaspari G 2004 *Elements of the Random Walk* (Cambridge: Cambridge University Press)
- [3] Spitzer F 1964 *Principles of Random Walk* (New York: Springer)
- [4] Feller W 1971 *An Introduction to Probability Theory and Its Applications* vol 2, 2nd edn (New York: Wiley)
- [5] Andersen E S 1962 The equivalence principle in the theory of fluctuations of sums of random variables *Colloquium on Combinatorial Methods in Probability Theory, Aarhus* pp 13–16
- [6] Gnedenko B V and Kolmogorov A N 1954 *Limit Distributions for Sums of Independent Random Variables* (Reading, MA: Addison-Wesley)
- [7] Zeller C and Cordery R 2020 Light scattering as a Poisson process and first-passage probability *J. Stat. Mech.* **2020** 063404
- [8] Zeller C and Cordery R 2024 First-return statistics in bounded radiative transport: A Motzkin polynomial framework *Preprint* arXiv:2512.13986v2
- [9] Kubelka P and Munk F 1931 *Z. Tech. Phys.* **12** 593–601
- [10] Chandrasekhar S 1960 *Radiative Transfer* (New York: Dover)
- [11] Sandoval C and Kim A D 2014 Deriving Kubelka–Munk theory from radiative transport *J. Opt. Soc. Am. A* **31** 628–636
- [12] Sandoval C and Kim A D 2017 Generalized Kubelka–Munk approximation for multiple scattering of polarized light *J. Opt. Soc. Am. A* **34** 153–162
- [13] Myrick M L, Simcock M N, Baranowski M, Brooke H, Morgan S L and McCutcheon J N 2011 The Kubelka–Munk diffuse reflectance formula revisited *Appl. Spectrosc. Rev.* **46** 140–165
- [14] Henyey L G and Greenstein J L 1941 Diffuse radiation in the galaxy *Astrophys. J.* **93** 70–83
- [15] Petnikova V M, Shuvalov V V and Tret’akov E V 2007 Multiple-scattering Henyey–Greenstein phase function and fast path-integration *Proc. SPIE* **6729** 672726
- [16] Pfeiffer N and Chapman G H 2008 Successive order, multiple scattering of two-term Henyey–Greenstein phase functions *Opt. Express* **16** 13637–13645

- [17] Oste R and Van der Jeugt J 2015 Motzkin paths, Motzkin polynomials and recurrence relations *Electron. J. Combin.* **22**(2) P2.8
- [18] Drake D and Gantner R 2011 Generating functions for plateaus in Motzkin paths *Preprint* arXiv:1109.3272
- [19] Simon K and Trachsler B 2003 A random walk approach for light scattering in material *Discrete Math. Theor. Comput. Sci.* pp 289–300
- [20] Sloane N J A 2023 A handbook of integer sequences fifty years later *Preprint* arXiv:2301.03149
- [21] Condamin S, Bénichou O and Moreau M 2005 First-passage times for random walks in bounded domains *Phys. Rev. Lett.* **95** 260601
- [22] Blanco S and Fournier R 2006 Short-path statistics and the diffusion approximation *Phys. Rev. Lett.* **97** 230604
- [23] Borovkov A A and Borovkov K A 2008 *Asymptotic Analysis of Random Walks: Heavy-Tailed Distributions* (Cambridge: Cambridge University Press)
- [24] De Bruijn N G 1981 *Asymptotic Methods in Analysis* 3rd edn (New York: Dover)
- [25] McDonald D R 1999 Asymptotics of first passage times for random walk in an orthant *Ann. Appl. Probab.* **9**(1) 110–145
- [26] Bouchaud J-P and Georges A 1990 Anomalous diffusion in disordered media: statistical mechanisms, models and physical applications *Phys. Rep.* **195** 127–293
- [27] Jacques S L 2010 Monte Carlo modeling of light transport in tissue (steady state and time of flight) *Optical-Thermal Response of Laser-Irradiated Tissue* 2nd edn (Berlin: Springer) pp 109–144
- [28] Sassaroli A, Blumetti C, Martelli F, Alianelli L, Contini D, Ismaelli A and Zaccanti G 1998 Monte Carlo procedure for investigating light propagation and imaging of highly scattering media *Appl. Opt.* **37** 7392–7400
- [29] Jacques S L 2013 Optical properties of biological tissues: a review *Phys. Med. Biol.* **58** R37–R61
- [30] Modrić D, Bolanča S and Beuc R 2009 Monte Carlo modeling of light scattering in paper *J. Imaging Sci. Technol.* **53** 020201